Cost-effective functionalization of Vulcan XC-72 by using the intermittent microwave heating process as nanocatalyst support for ethanol electrooxidation in acid media

W.J. Pech-Rodríguez, F.J. Rodríguez-Varela, E. Rocha-Rangel, D. González-Quijano, J.C. Martínez-Loyola, G. Vargas-Gutiérrez, G. Suarez-Velazquez, C. Morais, Teko Napporn

Vol. 20, No. 2 (2021) 955-973
Revista Mexicana de Ingeniería Química

Cost-effective functionalization of Vulcan XC-72 by using the intermittent microwave heating process as nanocatalyst support for ethanol electrooxidation in acid media

Funcionalización rentable del Vulcan XC-72 por medio de un proceso de calentamiento intermitente por microondas como soporte de nanocatalizador para la reacción de oxidación de etanol en medio ácido

W. J. Pech-Rodríguez[1]*, F.J. Rodríguez-Varela[2], E. Rocha-Rangel[1], D. González-Quijano[3], J. C. Martínez-Loyola[2], G. Vargas-Gutiérrez[2], G. Suarez-Velazquez[1], C. Morais[4], T.W. Napporn[4]

[1]*Departamento de Maestría en Ingeniería, Universidad Politécnica de Victoria, Ciudad Victoria, México.*
[2]*Sustentabilidad de los Recursos Naturales y Energía, Cinvestav Unidad Saltillo, Av. Industria Metalúrgica 1062, Ramos Arizpe, Coahuila, C.P. 25900, México.*
[3]*Departamento de Ingeniería Biomédica, Centro de Ciencias de la Ingeniería, Universidad Autónoma de Aguascalientes Campus Sur, Aguascalientes, México.*
[4]*Université de Poitiers, UMR 7285 CNRS, Equipe SAMCat, 4, Rue Michel Brunet, B27, TSA 51106, 86073 Poitiers Cedex 09, France.*

Received: January 27, 2021; Accepted: March 25, 2021

Abstract

Vulcan XC-72 samples were functionalized with methanol (MeOH) by the Intermittent Microwave Heating (IMH) under different treatment conditions. To assess the effectiveness of the proposed method, citric acid (CA) functionalization was also performed as comparison. The effectiveness of the surface treatment of the carbonaceous materials was assessed by using them as support for Pt/C-MeOH and Pt/C-CA nanocatalysts and conducting investigations of their catalytic activity for the Ethanol Oxidation Reaction (EOR). FTIR characterization reveals that Pt/C-MeOH was mainly composed of C-O, CH_3 and OH functional groups while Pt/C-CA presents more C-O species. The most active nanocatalyst was Pt/C-MeOH2 (0.15 mol L^{-1} MeOH and 8 min heating) which generated a current of 63.7 mA cm^{-2}. In situ SPAIRS measurements showed that the EOR at Pt/C-MeOH2 follows a C2-pathway mechanism where acetaldehyde is further oxidized to acetic acid, resulting in a high current density (j) generated from the EOR. Meanwhile, a competition between the C1 and C2 pathway was observed at Pt/C. The study demonstrated that the proposed IMH functionalization of Vulcan with MeOH produces carbon supported Pt nanocatalysts with enhanced catalytic activity for the EOR, with potential application in Direct Ethanol Fuel Cells (DEFC). Also, we believe that this simple and cost-effective green methanol functionalization can open opportunities to for the rational design of alloyed nanostructures useful in other areas of catalysis.

Keywords: Green vulcan surface functionalization, microwave heating, Pt/C nanocatalysts, in situ SPAIRS analysis, ethanol oxidation reaction.

Resumen

Las muestras de Vulcan XC-72 fueron funcionalizadas con metanol (MeOH) por medio de un calentamiento intermitente por microondas (IMH), utilizando diferentes condiciones. Para evaluar la efectividad del método propuesto también se llevó a cabo la funcionalización con ácido cítrico (CA). La efectividad del tratamiento superficial de los materiales carbonosos se evalúo al utilizarlos como soportes para los nanocatalizadores Pt/C-MeOH y Pt/C-CA y realizando también investigaciones de su actividad catalítica para la reacción de oxidación de etanol (EOR). La caracterización por espectroscopia infrarroja por transformada de Fourier (FTIR) muestra que el material Pt/C-MeOH estaba compuesto principalmente de grupos funcionales de C-O, CH_3 y OH mientras que el material Pt/C-CA presenta principalmente especies C-O. El nanocatalizador más activo fue Pt/C-MeOH2 (0.15 mol L^{-1} MeOH y 8 minutos de calentamiento) el cual generó una corriente de 63.7 mA cm^{-2}. Las mediciones in situ de SPAIRS mostraron que la EOR en el material Pt/C-MeOH sigue el mecanismo de la vía C2 donde el acetaldehído es oxidado a ácido acético, lo cual resulta en una alta densidad de corriente (j) debido a la EOR. Mientras tanto en el material Pt/C se observó una competencia entre las vías C1 y C2. El estudio demostró que la funcionalización propuesta con metanol y asistido por IMH para el carbón Vulcan produce un soporte carbonoso para los nano-catalizadores de Pt el cual mejora la actividad catalítica para la EOR, con una aplicación potencial en las celdas de consumo directo de etanol (DEFC). Además creemos que esta funcionalización con metanol rentable y verde puede abrir oportunidades para el diseño racional de nanoestructuras aleadas útiles en otras áreas de catálisis.

Palabras clave: funcionalización verde de la superficie del carbón Vulcan, calentamiento por microondas, nanocatalizadores Pt/C, análisis in situ SPAIRS, reacción de oxidación de etanol.

*Corresponding author. *E-mail*: wpechr@upv.edu.mx
https://doi.org/10.24275/rmiq/Cat2346
ISSN:1665-2738, *issn-e*: 2395-8472

1 Introduction

Fuel cells are attractive electrochemical devices for sustainable electric energy generation (Lindorfer, Rosenfeld, & Böhm, 2020; Paul, Saha, Qi, Stumper, & Gates, 2020; Shao, Dodelet, Wu, & Zelenay, 2019). These systems convert the chemical energy of a fuel (hydrogen, ethanol, methanol and others) into electricity via electrochemical reactions activated by nanocatalysts (Goor, Menkin, & Peled, 2019; Ioroi, Siroma, Yamazaki, & Yasuda, 2019; Rivera-Lugo *et al*., 2020; Y. Wang, Ruiz Diaz, Chen, Wang, & Adroher, 2020; Wnuk & Lewera, 2020). Up to present days, because of their high performance, noble metals have been used as efficient catalyst for fuel cells despite their cost (Esfandiari, Kazemeini, & Bastani, 2016; L. Wang *et al*., 2017). Nevertheless, for practical fuel cell applications it is required to develop active, stable and low-cost nanocatalysts (Ghosh, Bhandary, Basu, & Basu, 2017).

Pt based electrocatalysts are the most popular anodes in DEFC. However, these devices have a big challenge, because of the complexity of their oxidation at low temperatures, which includes C-C bonds cleavage not easy to occur at such operating conditions (S. Q. Song *et al*., 2005). Indeed, it is reported that Pt is one of the best electrocatalysts for the EOR in acid media, and its structure and morphology play a key role during the adsorption and oxidation of this alcohol(W. J. Zhou *et al*., 2004).

Meanwhile, the use of carbonaceous conductive materials as support have the purpose of reducing the metal loading and therefore the costs, also having a positive effect in promoting the catalytic activity of fuel cell nanocatalysts (Auer, Freund, Pietsch, & Tacke, 1998; Thompson, Jordan, & Forsyth, 2001). Carbon supports possess high surface area, good electrical conductivity and reasonable porosity (Dessources, del Jesús González-Quijano, & Pech-Rodríguez, 2018; Ghosh, Remita, *et al*., 2015; J. Wang *et al*., 2007). The support also enhances the metal utilization coefficient, while at the same time prevents aggregation and dissolution of metal nanoparticles (Ghosh, Bera, Bysakh, & Basu, 2017; Ghosh, Teillout, *et al*., 2015). A great deal of experimental studies of the EOR using Pt supported on carbonaceous materials has been carried out. For instance, ordered mesoporous carbon support was used to elucidate the effect of some templates in the electroactivity of Pt nanoparticles for alcohol oxidation (He *et al*., 2011). Pt/C suffers a poisoning effect due to the strong adsorption of CO, one of the main reaction intermediate, which diminished the availability of active sites for ethanol adsorption and oxidation. The EOR was studied in detail by using DEMS and in situ FTIR measurements, revealing that CO electrooxidation initiates at higher potentials at Pt/C compared with other nanomaterials such as $PtSnO_2$/C (Bach Delpeuch, Maillard, Chatenet, Soudant, & Cremers, 2016).With the aim to improve the electrocatalytic activity of Pt, different attempts have been made. One of them is the incorporation of a second or third element into the Pt structure. For instance, novel Pt/Re/SnO_2/C nanocatalysts were synthesized using a carbon support previously treated with HNO_3 and H_2O. The ternary material showed high catalytic activity and stability for the EOR (Drzymała *et al*., 2020).

Typically, carbon supports are normally pre-treated with the aim of promoting metal/support interactions forming surface functional groups and enhancing the catalytic activity of fuel cell nanocatalysts. Nowadays, great attention has been paid in the development of simple and versatile process for carbon functionalization to be used as support for noble metals and even as metal-free catalysts (Y. J. Yang & Li, 2014).

The most used carbon modification is the acid chemical functionalization (Guha, Lu, Zawodzinski, & Schiraldi, 2007; W. J. Pech-Rodríguez, González-Quijano, Vargas-Gutiérrez, & Rodríguez-Varela, 2014). In such process, carbon materials are treated in a concentrated solution of H_2SO_4 and HNO_3 under refluxing conditions followed by washing and filtering. Another method to functionalize carbon nanostructures is the citric acid (CA) treatment. Poh and coworkers have developed an effective method to functionalize carbon nanotubes by mixing them with CA, heating the solution at 300°C for 30 min (Poh, Lim, Pan, Lin, & Lee, 2008). The procedure successfully introduces HCOO- groups on the carbon surface, which create active sites for the nucleation and growth of well dispersed Pt nanostructures. The authors report that the functionalized Pt/C electrocatalyst enhances the current density of the Methanol Oxidation Reaction (MOR) in 0.5 mol L^{-1} H_2SO_4, attributed to a better Pt dispersion that promoted the removal of COads.

Also, Jiang and coworkers propose the functionalization of carbon nanotubes by using an HF/H_2O_2 mixture under IMH treatment (Yin, Shen, Song, & Jiang, 2009). The procedure consists

of several time-consuming steps where acetone, NaOH and HF are agents used to chemically treat the carbonaceous material. The Pt/CNT catalysts synthesized by this fashion show higher surface area, Pt utilization and catalytic activity for the Oxygen Reduction Reaction compared to other materials studied. Moreover, the use of soft chemical treatments of carbonaceous materials has been reported as well. For example, Yin and coworkers report the treatment of CNTs with KOH, followed by IMH at a temperature higher than 900°C and their application as support of Pt nanostructures (Yin *et al*., 2012). Such nanostructured catalyst shows a higher performance for the MOR than other Pt-based anodes. Recently, a two-step functionalization of nitrogen-doped carbon nano-onion has been reported. First, the carbon nanostructure has been refluxed in nitric acid and hydrogen peroxide for 6 h. Then, nitrogen doping has been performed by treating the sample with ammonia at 600 °C for 1 h (Sikeyi *et al*., 2021). Another procedure has been published by Zhang and coworkers, where CNTs have been successfully functionalized by using poly(diallyldimethyl ammonium) chloride as source of nitrogen (X. Zhang, Yang, & Jiang, 2021). Nevertheless, from the aforementioned works, it can be concluded that carbon functionalization has been traditionally achieved by using time-consuming processes where specialized equipment or costly chemical reagents are used.

This exploratory work reports a novel green procedure to functionalize Vulcan XC-72 using MeOH and CA as soft chemical agents, and the IMH process. The functionalized carbons are used as support for synthesizing Pt nanocatalysts by the microwave-assisted polyol method. The catalytic activity of the Pt nanoanodes supported on functionalized Vulcan for the EOR in acid media is compared to that of a conventional Pt/C nanocatalyst. The reaction mechanism of the EOR on some of the nanocatalysts is corroborated by in situ Single Potential Alteration IR Reflectance Spectroscopy (SPAIRS) analysis.

2 Materials and methods

2.1 Carbon functionalization

Vulcan® XC-72 (from now on Vulcan, Cabot Corp.) with a specific surface area of 237 m^2 g^{-1} was chemically modified with MeOH and CA (Sigma-Aldrich) as soft chemical reagents. The concentration of MeOH and CA used in this work was determined based on previous studies in our Laboratory (0.15 mol L^{-1} for MeOH and 0.05 mol L^{-1} for CA with two different times of functionalization: 4 and 8 min. As an example, the procedure to carry out the Vulcan functionalization to obtain C-MeOH1 was as follows: 300 mg of Vulcan were mixed by ultrasound in 30 mL of 0.15 mol L^{-1} MeOH for 1 h. The slurry was placed in a modified microwave oven and heated at ca. 100 °C, using a sequence of 25 s power on followed by 15 s power off under magnetic stirring, for 4 min of total irradiation time. The resulted solution was allowed to cool down for 1 h, vacuum filtered by using a PVDF membrane (0.45 μm pore size) and dried at 200 °C for 30 min, with the aim to remove all traces of the chemical reagent. C-MeOH2 was obtained by using 8 min of total irradiation. Thus, CA1 and CA2 where obtained after heat treatment at 4 and 8 min.

2.2 Synthesis of the Pt/C nanocatalysts

Anode materials with a nominal 20 wt. % Pt loading were synthesized by the IMH polyol method as described previously (W.J. Pech-Rodríguez, Gonzalez-Quijano, Vargas-Gutierrez, Escalante-Garcia, & Rodriguez-Varela, 2014). For example, 56 mg of modified Vulcan were dispersed by ultrasound in an EG/H_2O solution (v/v= 90/5) and 37 mg of $H_2PtCl_6{\cdot}6H_2O$ (Sigma-Aldrich) dispersed also in an EG/H_2O mixture were added drop by drop. The colloidal solution was stirred for 1 h, with the pH adjusted to 12 using a NaOH/EG solution. Afterwards, the sample was placed in the microwave oven and a radiation was applied continuously for 58 s, followed by pulses of 4 s power on and 15 s power off for a total time of 40 min. The mixture was left to cool at room temperature overnight with continuous stirring. Then, the pH was adjusted to 3 using an H_2SO_4/EG solution. The obtained product was filtered as described in the previous paragraph and washed with abundant deionized water.

2.3 Physicochemical characterization of the nanocatalysts

The synthesized nanocatalysts were characterized by XRD in a Phillips-X'Pert diffractometer using a CuKα radiation source with an working voltage of 40 kV, in a range between 10 and 100° (2θ). The chemical composition of the nanocatalysts was determined as the average of several measurements over the powder

sample, by using EDS in a Phillips XL30 SEM microscope operating at 20 kV. In order to identify the chemical functional group formed on their surface, some Vulcan samples were analyzed by FTIR in a Magna Nicolet 550 FTIR apparatus. Spectra were taken in the transmission mode with a resolution of 4 cm^{-1} in the scan range of 4000-500 cm^{-1} using KBr pellets (i.e., 120 mg of KBr were mixed with 0.8 mg of carbon).

Moreover, due to constraints in the use of the apparatus at our institutions, only two of the nanocatalysts were characterized in a HR-TEM Talos F200X microscope at an accelerating voltage of 200 kV, as well as in a Thermo Scientific K-Alpha+ XPS apparatus equipped with a monochromator (Al-Kα radiation, hv=1486.68 eV).

2.4 *Electrochemical characterization*

The experiments were performed in a three-electrode cell (Pine Inst.) using a Voltalab PGZ 301 potentiostat/galvanostat. The working electrode was obtained by transferring 10 μL of a catalytic ink, composed by 5 mg of the synthesized electrocatalyst in a solution of 0.5 mL isopropyl alcohol and 25 μL Nafion®, on a glassy carbon disc (0.5 mm). The counter electrode was a platinum sheet contained in a separate reservoir having a membrane at the tip. The reference electrode was of the Ag/AgCl type placed in a Luggin capillary also with a membrane at the tip. Nevertheless, all potentials reported in this work were referenced to the Reversible Hydrogen Electrode (RHE) scale. Cyclic voltammograms (CVs) were obtained in N_2-saturated 0.5 mol L^{-1} H_2SO_4 electrolyte at 20 mV s^{-1}.

The Electrochemically Active Surface Area (ECSA) of the materials was determined by integrating the charge associated to the average area of the hydrogen adsorption and desorption peaks, from the CVs. The catalytic activity for the EOR was evaluated in the same acid electrolyte containing 0.5 mol L^{-1} C_2H_5OH. The ethanol solution was added to the electrolyte while maintaining the working electrode under no polarization. Chronoamperometric measurements were conducted at 20 mV s^{-1}, polarizing the working electrode at 0.87 V vs. RHE in N_2-saturated 0.5 mol L^{-1} H_2SO_4 + 0.5 mol L^{-1} C_2H_5OH electrolyte.

2.5 *In situ FTIR characterization*

These measurements were carried out in a modified Bruker IFS 66V spectrometer with a resolution of 4 cm^{-1}. A three-electrode cell with transparent window (CaF2) was used. The working electrode was a disk of glassy carbon (8 mm diameter) that was modified by transferring 3 μL of the as prepared catalytic ink. The working electrode was activated by submitting them to 40 cycles at 40 mV s^{-1}. The ethanol solution was added to the electrolyte while maintaining the working electrode under no polarization. The Single Potential Alteration IR Spectroscopy (SPAIRS) was studied in a windows potential of 0.05 to 1.2 V vs. RHE. The electrode reflectivity REi was obtained at different potentials separated by 0.1 V with a sweep rate of 1 mV s^{-1}.

3 Results and discussion

Figure 1 shows the XRD patterns of Pt/C and the nanocatalysts obtained using Vulcan functionalized with MeOH and CA. The diffractogram of Pt/C shows a diffraction peak close to 25° that is ascribed to the (002) reflection of the graphite structure of Vulcan. The reflections located at 39.7, 46.2, 67.6 and 81.8° are attributed to the (111), (200), (220) and (311) planes of face-centered cubic Pt, respectively (JCPDF # 04-0802) (Silva *et al.*, 2010).

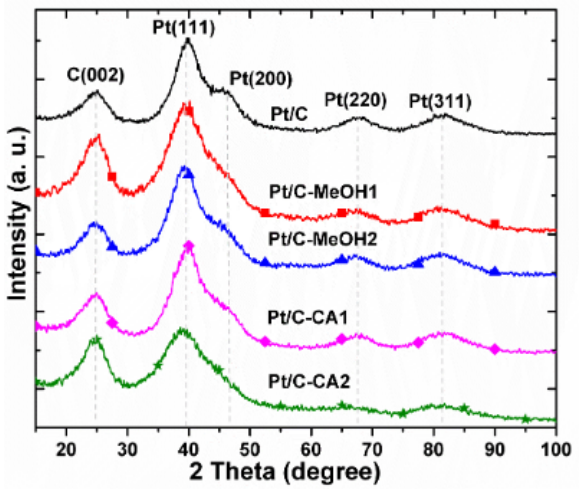

Fig. 1. XRD patterns of Pt/C and the nanocatalysts supported on Vulcan functionalized with MeOH and CA.

Table 1. Physical and chemical characteristics of the nanocatalyst.

Nanocatalyst	*d*, XRD (nm)	*d*, TEM (nm)	Pt content (wt.%)	ECSA (m^2g^{-1}
Pt/C	2.1	–	20.6	59.6
Pt/C-MeOH1	1.5	–	17.7	63.7
Pt/C-MeOH2	1.7	1.8	18.6	62.8
Pt/C-CA1	2.0	1.9	20.8	48.2
Pt/C-CA2	–	–	17.9	53.5

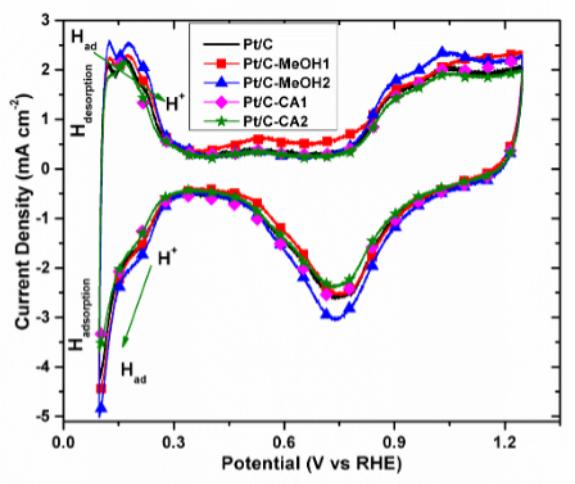

Fig. 2. Figure 2. CVs of Pt/C and the Pt/C-MeOH and Pt/C-CA series of nanocatalysts, obtained in N_2-saturated 0.5 mol L^{-1} H_2SO_4 at 20 mV s^{-1}.

Even though some similarities remain, changes emerge at the Pt/C-CA and the Pt/C-MeOH series of nanocatalysts compared to Pt/C, i.e., lower intensity, widening and shift in the position of some peaks as a result of the surface modification of Vulcan. Such differences can be attributed to the interaction of Pt nanoparticles with the treated carbon during their nucleation and growth. Changes in patterns can be more readily seen in the (220) plane.

The crystallite size of the nanocatalysts (*d*) is estimated from data of the (220) Pt plane using the Scherrer Equation (Hsu & Tongol, 2013):

$$d = \frac{0.9 \times \lambda}{\beta_{2\theta} \times \cos\theta} \quad (1)$$

where d is the average crystallite size, 0.9 is a shape factor for spherical crystallites, λ the radiation wavelength, $\beta_{2\theta}$ is the Full Width at Half Maximum and θ the position of the reflection peak.

Table 1 summarizes d values of 2.1 nm and less of the nanocatalysts. Pt/C-MeOH1 and Pt/C-MeOH2 have d= 1.5 and 1.7 nm, respectively, while in the case of Pt/C-CA2 it is not possible to calculate it because of the low intensity of the reflection. Table 1 also shows the Pt content at the nanoanodes, in all cases fairly close to the 20 wt. % nominally expected.

Figure 2 shows the CVs of Pt/C, along with the Pt/C-MeOH and Pt/C-CA series of nanocatalysts. Even though the curves have similar characteristics in terms of shape and *j*, Pt/C-MeOH2 shows a slightly higher intensity in the peaks corresponding to hydrogen adsorption/desorption, and formation/reduction of Pt-oxides. Pt/C-MeOH1 shows a more intense shoulder in the double layer region characteristic of the formation of hydroquinone species at Vulcan.

The ECSA values of the materials from the CVs in Figure 2 and after correction for double layer contributions have been determined using Equation (2):

$$ECSA = \frac{Q[\mu C\ cm^{-2}]}{Q_0[\mu C\ cm^{-2}Pt] \times Pt_{load}[mg\ cm}^{-2} \times 10^{-2} \quad (2)$$

where Q is the average electronic charge due to the adsorption and desorption of hydrogen; Q0 is the theoretical charge due to the adsorption of a monolayer of hydrogen on polycrystallite Pt (210 μC cm^{-2}) (Yin *et al.*, 2009); and Ptload is the amount of Pt on the working electrode, from data in Table 1. Pt/C has an ECSA value of 59.6 m^2 g^{-1} (Table 1). Nanocatalysts such as Pt/C-MeOH1 and Pt/C-MeOH2 show higher ECSA (e.g., 63.7 m^2 g^{-1} in the case of Pt/C-MeOH1). These nanocatalysts supported on methanol-functionalized Vulcan seem to have a surface that promote the utilization of the Pt nanoparticles. The polarization curves of the EOR at the nanocatalysts are shown in Figure 3 a). The anodes that generate higher *j* values with the reaction starting at more negative E_{onset} (0.3 V vs. RHE) are Pt/C-MeOH2 and Pt/C-CA1 (63.7 and 63.1 mA cm^{-2}, respectively), as seen in Table 2. The *j* value at Pt/C-MeOH2 and Pt/C-CA1 is roughly 1.2 times higher than that of Pt/C.

Table 2. Electrochemical parameters of the EOR at the nanocatalysts in 0.5 mol L^{-1} H_2SO_4.

Nanocatalyst	E_{onset} (V)	j (mA cm^{-2})	j at 0.55 V (mA cm^{-2})	j_m (mA mg_{Pt}^{-1})	j/j_b ratio
Pt/C	0.30	51.0	4.70	486.1	1.0
Pt/C-MeOH1	0.34	62.3	2.66	691.1	0.98
Pt/C-MeOH2	0.30	63.7	4.41	672.4	1.0
Pt/C-CA1	0.30	63.1	4.66	595.6	0.68
Pt/C-CA2	0.30	49.9	3.76	547.3	0.90

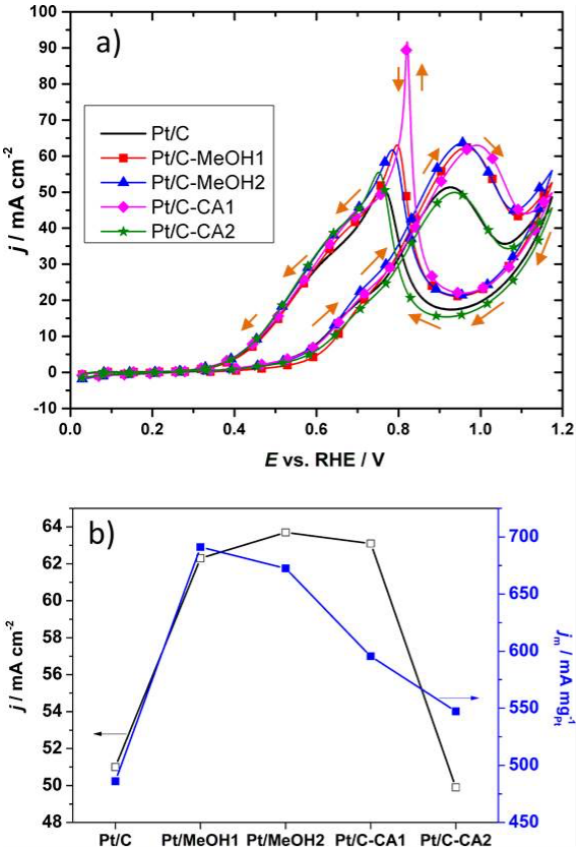

Fig. 3. XPS data of Pt/C-CA1 and Pt/C-MeOH2.

Pt/C-MeOH1 also generates higher j from the EOR than Pt/C, but at a more positive E_{onset}. In the Figure, there is a sharp increase in j at potentials around 0.55 V vs. RHE. At such potential, Pt/C and Pt/C-CA1 deliver slightly higher j values (4.70 and 4.66 mA cm^{-2}, respectively) than Pt/MeOH2, while Pt/C-MeOH1 and Pt/C-CA2 are less performing, as summarized in Table 2. These values show that Pt/C performs relatively well at the more negative potentials, but its behavior declines as the scan in the positive direction continues (as is also the case of Pt/C-CA2). Meanwhile, Pt/C-CA1, Pt/MeOH2 and Pt/C-MeOH1, show a better performance at the more positive potentials.

Figure 3 b) shows a plot of j and the peak mass current density (j_m, determined from the chemical composition obtained by EDS) at the nanocatalysts. It is clear that the performance of Pt/C-MeOH2, Pt/C-CA1 and Pt/MeOH1 is higher considering both geometric and mass activity, compared to Pt/C and Pt/C-CA2. Table 2 depicts the j_m values at each nanocatalyst. It can be seen that under this analysis, all the nanocatalysts supported on functionalized Vulcan generate a higher j_m than Pt/C, with values in the order Pt/C-MeOH1 > Pt/MeOH2 > Pt/C-CA1 > Pt/C-CA2 > Pt/C. The j values delivered by the functionalized Pt/C-MeOH nanocatalysts are superior or comparable with those reported in literature (G. Yang, Zhang, Yu, & Peng, 2021). For example, Song and coworkers synthesized a PtSnRh/C catalysts that exhibit j close to 20 mA cm^{-2} (S. Song *et al.*, 2012), a significantly lower value than the 63.7 mA cm^{-2} delivered by Pt/MeOH2.

Even more, an indication of the performance of the nanocatalysts to oxidize the organic molecule can be obtained by determining the ratio of current densities in the forward (j) and backward (j_b) scans (Liu, Ling, Su, & Lee, 2004; Scibioh *et al.*, 2008).

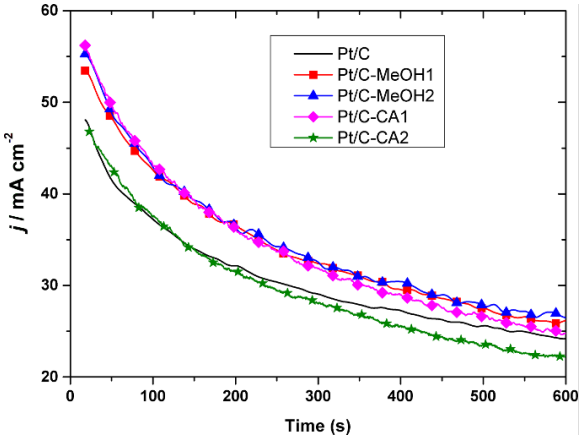

Fig. 4. Chronoamperometric curves of the EOR at the nanocatalysts. Applied potential 0.87 V vs. RHE in N_2-saturated 0.5 mol L^{-1} H_2SO_4 + 0.5 mol L^{-1} EtOH.

Under some conditions, Pt/C nanocatalysts show a j/j_b ratio close to 1 from the oxidation of organic molecules (Liu *et al*., 2004; Paul *et al*., 2020). Table 2 summarizes the j/j_b ratio of the nanocatalysts in this work. It is observed that Pt/MeOH2 has the same j/j_b ratio as that of Pt/C (i.e., 1.0), which is acceptable considering the fact that monometallic platinum is used for the oxidation of ethanol. Even though, it is acknowledged that Pt-alloys and Pt-metal oxide electrocatalysts can enhance the j/j_b ratio (Liu *et al*., 2004).

Figure 4 shows the chronoamperometric curves of the nanocatalysts. Pt/C-MeOH2, Pt/C-MeOH1 and Pt/C-CA1 have a more stable behavior and deliver a higher j after 600 s, which correlates with their performance in Figure 3. Pt/C and particularly Pt/C-CA2 show lower performance. The decay in j is related to the blockage of the active Pt sites mainly by CO species resulting from the partial dissociation of ethanol (Lu *et al*., 2019; C. Zhang, Zhu, Huang, Zhang, & Liu, 2014). Thus, it seems that Pt/C-MeOH2 has better capability to handle the CO poisoning effect and this can be due to the presence of functional groups or the modification of Pt state during the nucleation and growth at the functionalized carbon support. It is worth mentioning that the j value at the end of the study at Pt/C-MeOH2 is comparable with those reported elsewhere. For example, Zhang and coworkers report a j value close to 270 mA $mg^{-1}{}_{pt}$ from a PtNiRh NWs/C catalyst after chronoamperometric evaluation (W. Zhang *et al*., 2019), which is similar to 285 mA $mg^{-1}{}_{pt}$ at Pt/C-MeOH2 after the test.

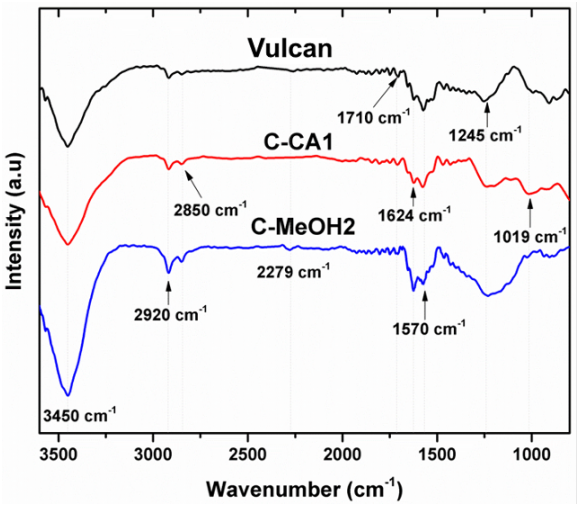

Fig. 5. FTIR spectra of untreated Vulcan, C-MeOH2 and C-CA1 (see Table 1 for functionalization conditions).

The higher performance of Pt/MeOH2 and Pt/CA1 in terms of j, j_m, as well as E_{onset}, compared to Pt/C (Pt/CMeOH1 generates a high j_m, but its E_{onset} is higher), suggests that the treatment of Vulcan with the soft MeOH and CA reagents under these conditions promotes the formation of surface functional groups (e.g., -COOH, C-O) that results in a homogeneous dispersion of Pt nanoparticles on the support. Figure 5 shows the representative FTIR spectra obtained from untreated Vulcan and the C-MeOH2 and C-CA1 treated samples.

The band located at 1019 cm^{-1} is due to the C-O stretching of the -COOH group (Lakshmi, Rajalakshmi, & Dhathathreyan, 2006) and as can be observed the C-CA1 sample displays a more intense peak compared to C-MeOH2 and Vulcan. This outcome is attributed to the fact that citric acid consists of 3 carboxyl groups. Moreover, the vibration due to the C-O groups (Figueiredo, Pereira, Freitas, & Órfão, 1999; Kuznetsova *et al*., 2000) is observed at 1245 cm^{-1} and is more intense at the treated carbons compared with the untreated one, i.e., more of these groups are there on the surface of C-CA1 and C-MeOH2. Also, an intense broad band between 1000 and 1492 cm^{-1} emerges at C-MeOH2, attributed to the contribution of C-O and CH_3 species (Ghobadi, Arami, Bahrami, & Mahmoodi, 2013; Vesali-Naseh *et al*., 2009; Wu, Hu, Shen, Li, & Wei, 2010; Y. J. Yang & Li, 2014). The bands at 1570 and 1710 cm^{-1} are due to C=O stretching vibrations (Vesali-Naseh *et al*., 2009; Wu *et al*., 2010) and as can be seen, C-CA1 and C-MeOH2 show different features in this region compared to Vulcan. It can also be observed that the band at 1624 cm^{-1}, due to the C=C stretching vibrations (Ghobadi *et al*., 2013; Moon, Park, Kim, & Choi, 2011), is more intense at the functionalized carbons.

The two peaks located at 2850-2920 cm^{-1} are ascribed to the C-H symmetric and asymmetric stretching vibrations (Ghobadi *et al*., 2013) and are more intense at C-MeOH2 and C-CA1. Even more, the band at 3450 cm^{-1} is ascribed to hydroxyl groups. From Figure 5, it can be seen that C-MeOH2 has an intense band in this region compared with the other samples, which can be explained by -OH groups formed at this material after functionalization with methanol (CH_3-OH) molecules. These features confirm that surface functional groups are formed at C-MeOH2 and C-CA1 after chemical treatment by IMH in the presence of methanol and citric acid, respectively. The successful incorporation of OH, C-O and CH_3 onto the carbon plays a key role because

these functional groups represent favorable sites for Pt ion adsorption, preventing the agglomeration of Pt into large nanoparticles (Youssry, Al-Ruwaidhi, Zakeri, & Zakeri, 2020). These results correlate well with the crystallite size determined from XRD analysis (Table 1).

The Pt/C-CA1 and Pt/C-MeOH2 nanocatalyst have been characterized by HR-TEM and XPS. It must be emphasized that access to the apparatus in our institutions is limited, therefore, only these two nanomaterials have been studied by these techniques. The image of Pt/C-CA1 in Figure 6 a) shows a high dispersion of Pt nanoparticles over the functionalized Vulcan.

From this micrograph, an average particle size (d) of 1.9 nm has been determined (Table 1), in good agreement with the XRD value. Moreover, the nanocatalyst has been submitted to High Angle Annular Dark Field (HAADF) analysis. Figure 6 b) confirms Pt nanoparticles homogeneously dispersed on the support, along with the chemical mapping highlighting the position of Pt, C and O sites. The excellent morphology at this nanocatalyst is advantageous, since well dispersed Pt nanoparticles leads to more active sites available for the dissociative chemisorption and further oxidation of ethanol molecules. This feature is also related to a higher electrochemically active surface area (ECSA).

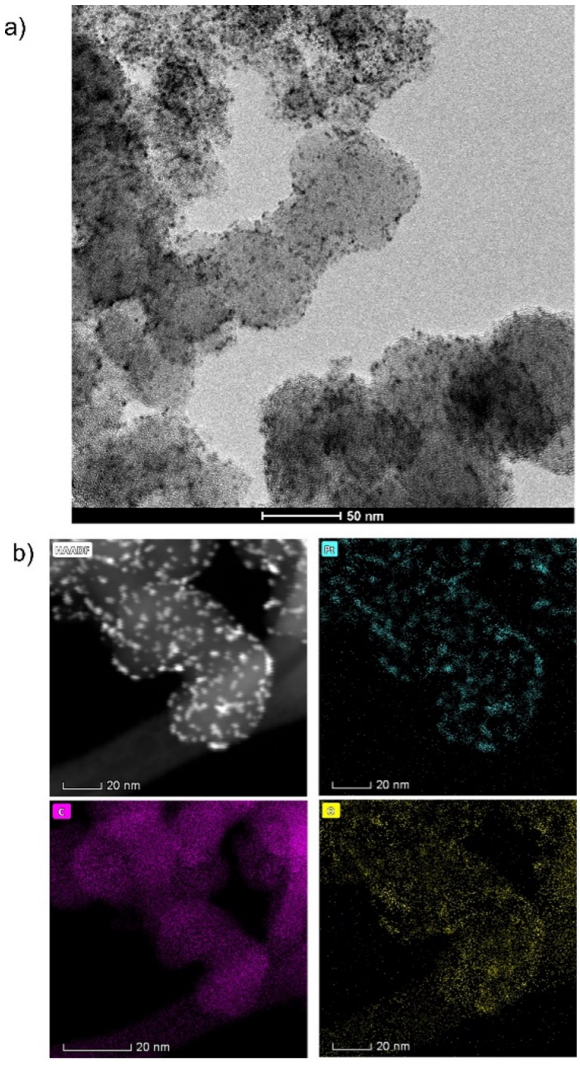

Fig. 6. a) HR-TEM image and b) HAADF characterization showing the chemical mapping of the Pt/C-CA1 nanocatalyst.

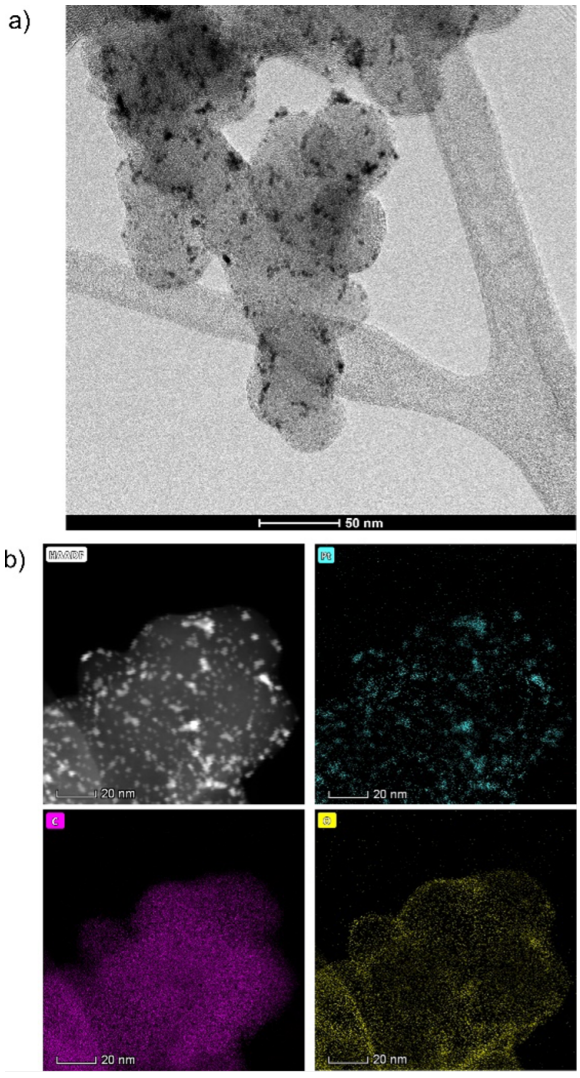

Fig. 7. a) HR-TEM image and b) HAADF characterization showing the chemical mapping of the Pt/C-MeOH2 nanocatalyst.

Moreover, the utilization factor becomes more important, since apparently spherical nanoparticles are formed by the IMH assisted polyol method. Opposed, agglomerated Pt nanoparticles have a smaller ECSA value and a great deal of active sites are not available for ethanol chemisorption.

The same characterization has been performed on Pt/C-MeOH2, which also shows a high dispersion of Pt nanoparticles on the functionalized support (Figure 7 a). The d value of this nanocatalyst is 1.8 nm (Table 1), similar to that obtained from XRD. Figure 7 b) shows its HAADF characterization, where the chemical mapping also demonstrates the excellent dispersion of Pt nanoparticles, along with the presence of C and O.

These features confirm the advantageous functionalization of Vulcan with CA and MeOH, which along with the well-known high capacity of the microwave-assisted polyol method to limit the particle size growth of fuel cell nanocatalysts, results in a homogeneous dispersion of Pt nanoparticles at Pt/C-CA1 and Pt/C-MeOH2.

Figure 8 shows the XPS spectra of the two nanocatalysts. In the C 1s region, signals attributed to carbon sp2 (C=C) and sp3 (C-C) hybridizations at a binding energy (BE) of 284.84 and 285.84 eV, respectively, are observed at Pt/C-CA1 (A. A. Siller-Ceniceros *et al.*, 2017). A peak due to C-O species (Adriana A. Siller-Ceniceros *et al.*, 2019) is also detected at a BE= 286.43 eV (Figure 8 a and Table 3).

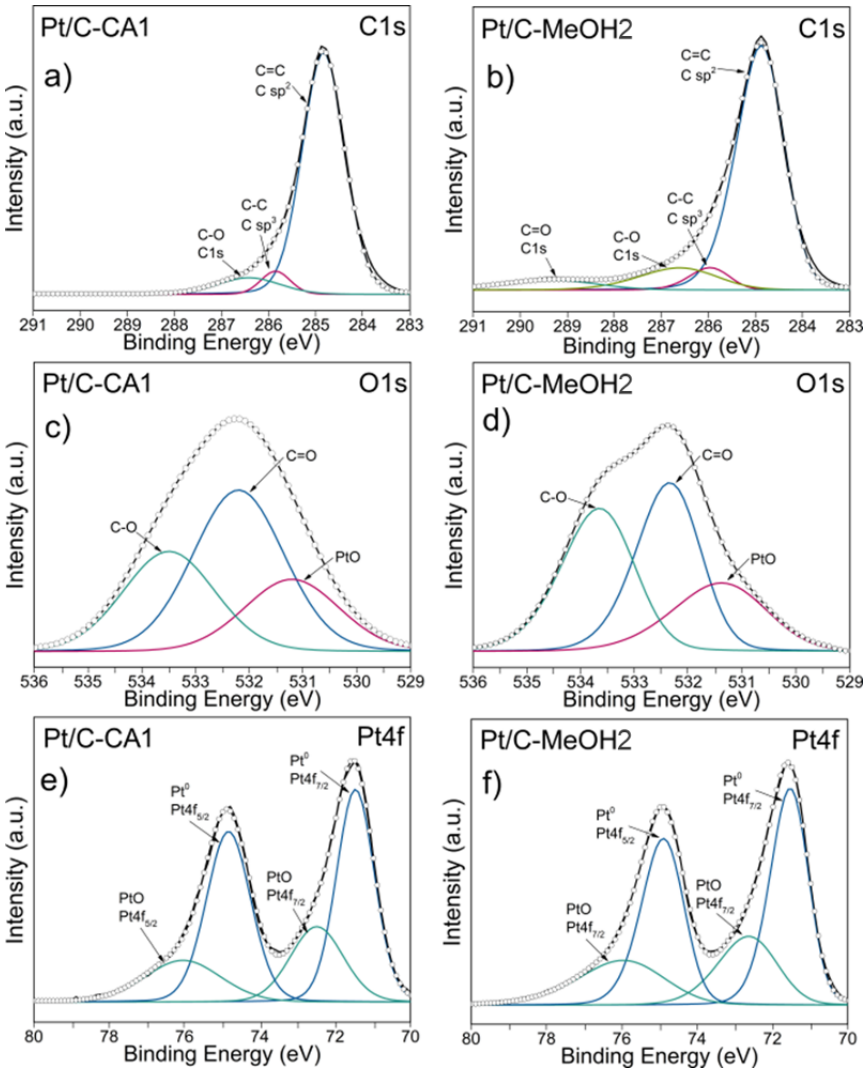

Fig. 8. XPS spectra of Pt/C-CA1 and Pt/C-MeOH2 at the regions: a-b) C 1s, c-d) O 1s, and e-f) Pt 4f.

Pt/C-MeOH2 shows these same signals, with slight shifts in BE (Figure 8 b and Table 3). Additionally, a clear peak due to C=O species at BE= 289.35 eV is observed in the spectrum of Pt/C-MeOH2 (Arteaga *et al*., 2019; Adriana A. Siller-Ceniceros *et al*., 2019; X. Wang *et al*., 2015), which is not detected at Pt/C-CA1. Such difference may be due to an effect of the functionalization with methanol. The higher C content at both nanocatalysts is that of sp2 (around 63-65 at. %, Table 3).

In the O 1s state, the nanocatalysts show C=O and C-O bonds, along with the formation of the PtO species (Figures 8 c and d). The presence of the C-O species has not been observed in our previous work on a similar Pt/C nanocatalyst supported on non-functionalized Vulcan (A. A. Siller-Ceniceros *et al*., 2017). Therefore, even though more studies can be performed in future work, such C-O peak is likely to be due to the functionalization of Vulcan with MeOH and CA.

Figures 8 e) and f) depict the signals at the Pt 4f region of Pt/C-CA1 and Pt/C-MeOH2, respectively. The splitting into the Pt4f7/2 and Pt4f5/2 states leads to doublets attributed to Pt0 and PtII (Li *et al*., 2013). The total Pt content is of 21.17 and 20.56 at. % on Pt/C-CA1 and Pt/C-MeOH2, respectively. The surface chemical composition of Pt/C-CA1 indicates 6.39 and 14.78 Pt0 and PtII (at. %), respectively. The values are 6.79 and 13.77 at. % in the case of Pt/C-MeOH2 (Table 3).

With the aim of gaining a better understanding of the effect of Vulcan treatment on the catalytic activity of the nanocatalysts for the EOR, SPAIRS measurements (from 0.1 V to 1.2 V, in 0.1 V intervals), have been conducted on Pt/C-CA1 and Pt/C-MeOH2 (the most active nanocatalysts) as well as on Pt/C-MeOH1, with Vulcan irradiated by IMH in half the time related to the first one. Pt/C, being a reference nanocatalyst, has also been characterized by this technique. Figure 9 shows the spectra obtained from a) Pt/C and b) Pt/C-CA1, while Figure 10 depicts those of a) Pt/C-MeOH1 and b) Pt/C-MeOH2. It is observed that starting at 0.3 V vs RHE, an IR band emerges at about 2050 cm^{-1}, corresponding to linearly adsorbed CO_L, species that form as a result of the ethanol dissociation step. The presence of such species can be associated to a reaction mechanism that follows a C1-pathway.

Table 3. XPS data of Pt/C-CA1 and Pt/C-MeOH2.

Nanocatalyst	Species	State	*BE* (eV)	Doublet splitting (eV)	Composition (at. %)
Pt/C-CA1	C=C	C 1s	284.84		65.15
	C-C	C 1s	285.84		3.49
	C-O	C 1s	286.43		2.53
	C=O	O 1s	532.19		6.45
	C-O	O 1s	533.5		1.21
	Pt^0	$Pt4f_{7/2}$	71.47	3.36	3.29
		$Pt\ 4f_{5/2}$	74.83		3.1
	PtO	$Pt\ 4f_{7/2}$	72.48	3.58	2.71
		$Pt\ 4f_{5/2}$	76.06		1.86
		O 1s	531.18		10.21
Pt/C-MeOH2	C=C	C 1s	284.83		63.42
	C-C	C 1s	285.96		3.59
	C-O	C 1s	286.62		2.46
	C=O	C 1s	289.35		1.98
	C=O	O 1s	532.33		5.38
	C-O	O 1s	533.66		2.61
	Pt^0	$Pt\ 4f_{7/2}$	71.52	3.38	3.41
		$Pt\ 4f_{5/2}$	74.9		3.38
	PtO	$Pt\ 4f_{7/2}$	72.73	3.21	2.65
		$Pt\ 4f_{5/2}$	75.94		1.89
		O 1s	531.35		9.23

This signal is clearly more intense at Pt/C as compared to Pt/C-CA3, Pt/C-MeOH5 and Pt/C-MeOH6, and remains almost unchanged as the potential rises. This is one of the reasons why the Pt/C material shows a lower catalytic activity for the EOR, since some of the Pt sites become poisoned by the C1-species. Additionally, the Pt/C and Pt/C-CA1 nanocatalysts display a clear band at 1640 cm^{-1} due to the bending vibration of water molecules (Almeida *et al.*, 2012; Palma *et al.*, 2014). Meanwhile the perturbation close to 1840 cm^{-1} is ascribed to the presence of bridge-bonded CO (Z.-Y. Zhou, Wang, Lin, Tian, & Sun, 2010).

The band at 2345 cm^{-1} is associated with the CO_2 anti-symmetric stretch vibration (W. J. Pech-Rodríguez *et al.*, 2017; Wnuk & Lewera, 2020) and it is observed at potentials starting at 0.7 V in Pt/C-CA1, Pt/C-MeOH1 and Pt/C-MeOH2. As can be seen in Figure 9 b), this band is more intense at Pt/C-CA1 compared to the other nanocatalysts.

The broad band centered at 2615 cm^{-1} may be ascribed to an overlapping of the C-H stretch vibration of acetaldehyde and the O-H stretch of the carboxyl group in acetic acid (Dos Anjos, Hahn, Léger, Kokoh, & Tremiliosi-Filho, 2007). Therefore, it is related to a C2-pathway mechanism of the EOR. Pt/C-CA1 and Pt/C-MeOH1 show a higher intensity of this band. Also, another band can be seen at 1709 cm^{-1}, which is ascribed to the stretch of the C=O carbonyl group both on acetaldehyde and acetic acid (De Souza *et al.*, 2012). Moreover, the bands at 1280 cm^{-1} and 1390 cm^{-1} are ascribed to the C-O stretch and O-H deformation vibrations in acetic acid (Camara & Iwasita, 2005; Lai *et al.*, 2010; Q. Wang *et al.*, 2007) while the bands at 1368 cm^{-1} and 1100 cm^{-1} are due to the symmetrical deformation of CH_3 and CH vibrating in acetaldehyde (Q. Wang *et al.*, 2007). The spectra also show the presence of upgoing bands at 1047 and 1088 cm^{-1} which are related to the consumption of ethanol (Geraldes *et al.*, 2013; Thotiyl, Kumar, & Sampath, 2010).

Further analysis of the EOR mechanism on the nanocatalysis is obtained from the intensities of the acetic acid (1280 cm^{-1}) and the CO (2050 cm^{-1}) bands, normalized by the integrated area of the CH3COH signals (1368 cm^{-1}) at a potential of 1.2 V, as shown in Figure 11. From Figure 11 a), it can be seen that Pt/C-CA1 has the lowest band intensity suggesting that acetaldehyde is mainly formed on this nanocatalyst (i.e., a 2 e- transfer). The large formation of acetaldehyde on Pt/C-CA1 may explain in part its low j/j_b ratio in Table 2.

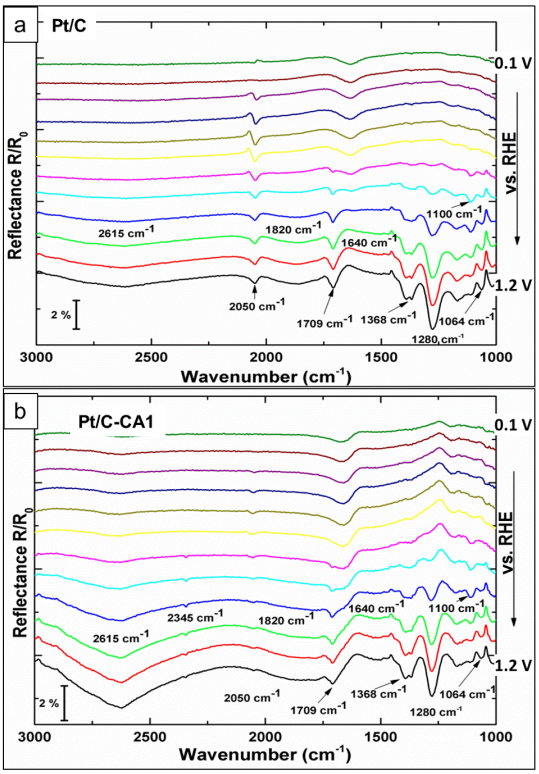

Fig. 9. In situ FTIR spectra of the EOR at the Pt/C and Pt/C-CA1 nanocatalysts in 0.5 mol L^{-1} H_2SO_4 + 0.5 mol L^{-1} EtOH.

It can also be correlated with the relatively high intensity of the CO_2 band at the nanocatalyst in Figure 9 b), which is produced according to reaction (1) [6]:

$$Pt{-}(CO)_{ads} + Pt{-}OH_{ads} \longrightarrow CO_2 + H^+ + 2Pt^+e^- \quad (3)$$

As can be seen, Pt/C and Pt/C-CA1 have the same trend, since their band intensity increases as the potential goes from 0.8 to 1.2 V. Nevertheless, the acetaldehyde yield at these two nanocatalysts is lower with respect to acetic acid.

Meanwhile, Pt/C-MeOH2 and Pt/C-MeOH1 have higher band intensity at potentials higher than ca. 0.95 V, confirming a higher acetic acid yield (i.e., a 4 e-transfer). Therefore, the high current density delivered particularly by Pt/C-MeOH2 is due to a mechanism involving the production of acetaldehyde and its oxidation to acetic acid (Rizo, Pérez-Rodríguez, & García, 2019).

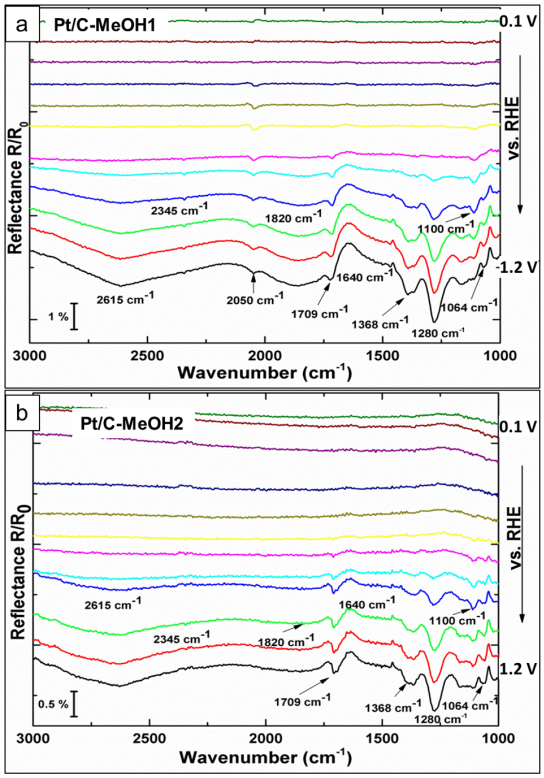

Fig. 10. In situ FTIR spectra of the EOR at the Pt/C-MeOH1 and Pt/C-MeOH2 nanocatalysts in 0.5 mol L^{-1} H_2SO_4 + 0.5 mol L^{-1} EtOH.

The high yield of acetic acid on Pt/C-MeOH2 and Pt/C-MeOH1 may be due to the presence of hydroxyl groups (ethoxy species) (Guillén-Villafuerte, García, Arévalo, Rodríguez, & Pastor, 2016), which promote the oxidation process, according to the following reaction (Lamy, Belgsir, & Léger, 2001):

$$(CH_3 - CHO)_{ads} + \text{Pt-OH}_{ads} \longrightarrow CH_3\text{-COOH} + H^+ + e^- + \text{Pt} \quad (4)$$

The low performance of Pt/C can also be explained by the fact that this nanocatalyst follows a complex multistep process where adsorbed acetaldehyde is further oxidized to CO and CH_3 adsorbed species (Lai *et al.*, 2010; Rizo *et al.*, 2019). As opposed to what has been discussed elsewhere (Rizo *et al.*, 2019), the CO and CH_3 groups formed at Pt/C do not react at the catalytic sites, i.e., no CO_2 is produced.

Figure 11 b) shows the normalized band intensities for the CO signal. From this Figure it is concluded that Pt/C produces a significantly higher amount of CO-species, while the treated electrocatalysts show lower intensities of this band. As can be seen in Figure 9 a), CO-species are clearly formed at Pt/C, but no band related to CO_2 formation is detectable. Evidently, C1 and C2 species are adsorbed on the catalytic surface of Pt/C, blocking its active sites that should promote the EOR.

The SPAIRS results in Figures 9 to 11 demonstrates that at Pt/C-MeOH2, Pt/C-MeOH1 and Pt/C-CA1, ethanol molecules undergo the breaking of C-C bonds and a dehydrogenation step, in a path that involves the formation of acetaldehyde and acetic acid. It has been reported that acetaldehyde and acetic acid contribute with 60% or higher of the current density generated during the EOR (Rizo *et al.*, 2019), which explains in part the higher values of *j* at these nanocatalysts compared to Pt/C in Table 2. On the other hand, it is to be noticed that Pt/C-CA1 forms a relatively high amount of CO_2, which is a relevant electrocatalytic behavior, considering that the overall conversion efficiency of C_2H_5OH to carbon dioxide has been reported to be of less than 6% (Flórez-Montaño *et al.*, 2016; Guillén-Villafuerte *et al.*, 2016).

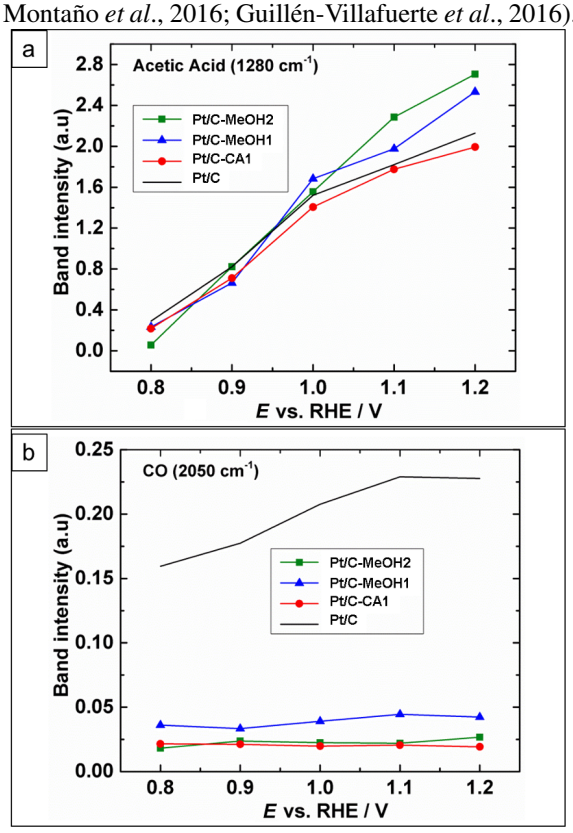

Fig. 11. Normalized band intensities of acetic acid and CO.

Table 4. Comparison of catalytic activity and stability of Pt/C-MeOH2 with those of several Pt-alloys reported in the literature.

Material	Composition (at. %)	Peak potential/scam rate	j	j at the end of chronoamperometry/applied potential/time of the test	Electrolyte	Reference
PtSn/C	2:01	0.740 V vs SCE 50 mV s^{-1}	61 mA cm^{-2}	-	1 mol L^{-1} C_2H_5OH + 1 mol L^{-1} $HClO_4$	(Song *et al.*, 2005)
PtRu/C	1:01	0.95 V vs NHE 25 mV s^{-1}	26 mA cm^{-2}	25 mA cm^{-2} 0.8 V for 10 min	1 mol L^{-1} C_2H_5OH + 0.5 mol L^{-1} $HClO_4$	(Li, Sun, Cao, Jiang, & Xin, 2007)
PtRuMo/C	63.7:26.2:10.1	0.92 V vs RHE @ 20 mV s^{-1}	31 mA cm^{-2}	8 mA cm^{-2} @ 0.8 V for 10 min	0.5 mol L^{-1} C_2H_5OH + 0.5 mol L^{-1} H_2SO_4	(Wang, Yin, & Lin, 2007)
PtSn/C	1.7:1	0.983 V vs RHE @ 20 mV s^{-1}	658.52 mA $mg^{-1}{}_{Pt}$	12 mA cm^{-2} 0.6 V for 10 min	0.5 mol L^{-1} C_2H_5OH + 0.5 mol L^{-1} H_2SO_4	(González-Quijano *et al.*, 2015)
PtNiRh	66:27:07	0.66 v vs SCE @ 50 mV s^{-1}	750 mA $mg^{-1}{}_{Pt}$	350 mA $mg^{-1}{}_{Pt}$ 0.65 V for 10 min	0.5 mol L^{-1} C_2H_5OH + 0.5 mol L^{-1} H_2SO_4	(Lu *et al.*, 2019)
PtNiCu/C	35.5:6.1:58.4	0.95 V vs RHE 50 mV s^{-1}	634 mA $mg^{-1}{}_{Pt}$	125 mA $mg^{-1}{}_{Pt}$ 0.74 V for 10 min	1 mol L^{-1} C_2H_5OH + 0.5 mol L^{-1} H_2SO_4	(Castagna, Sieben, Alvarez, Sanchez, & Duarte, 2020)
Pt/C-MeOH2	-	0.95 V vs RHE 20 mV s^{-1}	63.7 mA cm^{-2} or 672.4 mA $mg^{-1}{}_{Pt}$	27 mA cm^{-2} or 285 mA $mg^{-1}{}_{Pt}$ 0.87 V for 10 min	0.5 mol L^{-1} C_2H_5OH + 0.5 mol L^{-1} H_2SO_4	This work

A comparison of the catalytic activity of Pt/C-MeOH2 with that of some Pt-alloys from the literature is shown in Table 4. As can be observed, the nanocatalyst developed in this work shows a high performance for the EOR.

To the best of our knowledge, exploratory studies of the green surface functionalization of the widely used Vulcan support with soft agents such as MeOH and CA, using IMH, have not been reported before. More importantly, the positive effect that, under some experimental conditions, such functionalization has on the performance of Pt/C nanocatalysts for the EOR clearly indicates the road to perform more studies. For example, it is of interest to evaluate the effect of varying experimental parameters such as concentration of chemical agent and time of heating. The outcome is highly relevant for the development of active nanocatalysts for DEFC applications. The results shown in this work also open the opportunity to use the functionalized supports to disperse Pt-alloys (e.g., Pt-Sn/C) in future work.

Conclusions

The surface chemistry of commercial Vulcan XC-72 was effectively modified from the functionalization with MeOH and CA, using IMH. The HR-TEM average particle size of Pt/C-MeOH2 and Pt/C-CA1 was below 2 nm, indicating good anchorage and inhibition of particle size growth of Pt nanoparticles. Functionalization with MeOH promotes the formation of C=O bonds in Pt/C-MeOH2, a species not observed at Pt/C-CA1. Moreover, C-O species were formed at both nanocatalysts, not observed previously at non-functionalized Vulcan. From the SPAIRS measurements it was observed that Pt/C-MeOH2 and Pt/C-CA1 showed a higher catalytic activity for the EOR. The reaction mechanism followed a C2-pathway at these nanocatalysts. At Pt/C-MeOH2, acetic acid is preferentially formed. On the contrary, the mechanism follows a higher rate of acetaldehyde production at Pt/C-CA1. Both nanocatalysts showed a low generation of CO_L species.

Therefore, the results of this exploratory work indicated that green and rapid functionalization of Vulcan with MeOH and CA, using IMH, is a promising process for the development of highly active Pt nanocatalysts for the oxidation of ethanol in acid media.

Acknowledgements

This work was financially supported by the Mexican National Council for Science and Technology

(CONACYT) through grant 241526. We thank CONACYT for doctoral scholarships and support through the Programa de Becas Mixtas provided to WJPR and DGQ.

References

Almeida, T. S., Palma, L. M., Leonello, P. H., Morais, C., Kokoh, K. B., & De Andrade, A. R. (2012). An optimization study of PtSn/C catalysts applied to direct ethanol fuel cell: effect of the preparation method on the electrocatalytic activity of the catalysts. *Journal of Power Sources 215*, 53-62. doi: http://dx.doi.org/10.1016/j.jpowsour.2012.04.061

Arteaga, Gladys, Rivera-Gavidia, M. Luis, Martínez, J. Sthephanie, Rizo, Rubén, Pastor, Elena, & García, Gonzalo. (2019). Methanol oxidation on graphenic-supported platinum catalysts. *Surfaces 2*, 16-31. doi: http://dx.10.3390/surfaces2010002

Auer, E., Freund, A., Pietsch, J., & Tacke, T. (1998). Carbons as supports for industrial precious metal catalysts. *Applied Catalysis A: General 173*, 259-271. doi: http://dx.doi.org/10.1016/S0926-860X(98)00184-7

Bach Delpeuch, Antoine, Maillard, Frédéric, Chatenet, Marian, Soudant, Priscillia, & Cremers, Carsten. (2016). Ethanol oxidation reaction (EOR) investigation on Pt/C, Rh/C, and Pt-based bi- and tri-metallic electrocatalysts: a DEMS and in situ FTIR study. *Applied Catalysis B: Environmental 181*, 672-680. doi: https://doi.org/10.1016/j.apcatb.2015.08.041

Camara, G. A., & Iwasita, T. (2005). Parallel pathways of ethanol oxidation: the effect of ethanol concentration. *Journal of Electroanalytical Chemistry 578*, 315-321. doi: http://dx.doi.org/10.1016/j.jelechem.2005.01.013

Castagna, Rodrigo M., Sieben, Juan Manuel, Alvarez, Andrea E., Sanchez, Miguel D., & Duarte, Marta M. E. (2020). Carbon supported PtNiCu nanostructured particles for the electro-oxidation of ethanol in acid environment. *Materials Today Energy 15*, 100366-100375. doi: https://doi.org/10.1016/j.mtener.2019.100366

De Souza, R. F. B. , Silva, J. C. M., Simões, F. C. , Calegaro, M. L. , Neto, A. O. , & Santos, M. C. (2012). New approaches for the ethanol oxidation reaction of Pt/C on carbon cloth using ATR-FTIR. *International Journal of Electrochemical Science 7*, 5356 - 5366.

Dessources, Samuel, del Jesús González-Quijano, Diego Xavier, & Pech-Rodríguez, Wilian Jesús. (2018). Non-noble metal as catalysts for alcohol electro-oxidation reaction. In F. J. Rodríguez-Varela & T. W. Napporn (Eds.), *Advanced Electrocatalysts for Low-Temperature Fuel Cells* (pp. 263-290). Cham: Springer International Publishing.

Dos Anjos, D. M., Hahn, F., Léger, J. M., Kokoh, K. B., & Tremiliosi-Filho, G. (2007). In situ FTIRS studies of the electrocatalytic oxidation of ethanol on Pt alloy electrodes. *Journal of Solid State Electrochemistry 11*, 1567-1573. doi: https://doi:10.1007/s10008-007-0360-y

Drzymała, Elzbieta, Gruzeł, Grzegorz, Depciuch, Joanna, Pawlyta, Miroslawa, Donten, Mikołaj, & Parlinska-Wojtan, Magdalena. (2020). Ternary Pt/Re/SnO_2/C catalyst for EOR: electrocatalytic activity and durability enhancement. *Nano Research 13*, 832-842. doi: https://doi.org/10.1007/s12274-020-2704-1

Esfandiari, Ali, Kazemeini, Mohammad, & Bastani, Dariush. (2016). Synthesis, characterization and performance determination of an Ag@Pt/C electrocatalyst for the ORR in a PEM fuel cell. *International Journal of Hydrogen Energy 41*, 20720-20730. doi: https://doi.org/10.1016/j.ijhydene.2016.09.097

Figueiredo, J. L., Pereira, M. F. R., Freitas, M. M. A., & Órfão, J. J. M. (1999). Modification of the surface chemistry of activated carbons. *Carbon 37* 1379-1389. doi: http://dx.doi.org/10.1016/S0008-6223(98)00333-9

Flórez-Montaño, Jonathan, García, Gonzalo, Guillén-Villafuerte, Olmedo, Rodríguez, José Luis, Planes, Gabriel A., & Pastor, Elena. (2016). Mechanism of ethanol electrooxidation

on mesoporous Pt electrode in acidic medium studied by a novel electrochemical mass spectrometry set-up. *Electrochimica Acta 209*, 121-131. doi: https://doi.org/10.1016/j.electacta.2016.05.070

Geraldes, Adriana Napoleão, da Silva, Dionisio Furtunato, Pino, Eddy Segura, da Silva, Júlio César Martins, de Souza, Rodrigo Fernando Brambilla, Hammer, Peter,Spinace, Vitório Estevam, Neto Oliveira, Almir, Coelho dos Santos, Mauro. (2013). Ethanol electro-oxidation in an alkaline medium using Pd/C, Au/C and PdAu/C electrocatalysts prepared by electron beam irradiation. *Electrochimica Acta 111*, 455-465. doi: http://dx.doi.org/10.1016/j.electacta.2013.08.021

Ghobadi, Jalil, Arami, Mokhtar, Bahrami, Hajir, & Mahmoodi, Niyaz Mohammad. (2013). Modification of carbon nanotubes with cationic surfactant and its application for removal of direct dyes. *Desalination and Water Treatment 1*, 1-13. doi: https://doi.org/10.1080/19443994.2013.801790

Ghosh, Srabanti, Bera, Susmita, Bysakh, Sandip, & Basu, Rajendra Nath. (2017). Highly active multimetallic palladium nanoalloys embedded in conducting polymer as anode catalyst for electrooxidation of ethanol. *ACS Applied Materials & Interfaces 9*, 33775-33790. doi: https://doi.org/10.1021/acsami.7b08327

Ghosh, Srabanti, Bhandary, Nimai, Basu, Suddhasatwa, & Basu, Rajendra N. (2017). Synergistic effects of polypyrrole nanofibers and Pd nanoparticles for improved electrocatalytic performance of Pd/PPy nanocomposites for ethanol oxidation. *Electrocatalysis 8*, 329-339. doi: https://doi.org/10.1007/s12678-017-0374-x

Ghosh, Srabanti, Remita, Hynd, Kar, Prasenjit, Choudhury, Susobhan, Sardar, Samim, Beaunier, Patricia, Sarathi Roy, Partha, Bhattacharya, Swapan Kumar, Pal, Samir Kumar. (2015). Facile synthesis of Pd nanostructures in hexagonal mesophases as a promising electrocatalyst for ethanol oxidation. *Journal of Materials Chemistry A 3*, 9517-9527. doi: https://doi.org/10.1039/C5TA00923E

Ghosh, Srabanti, Teillout, Anne-Lucie, Floresyona, Dita, de Oliveira, Pedro, Hagège, Agnès, & Remita, Hynd. (2015). Conducting polymer-supported palladium nanoplates for applications in direct alcohol oxidation. *International Journal of Hydrogen Energy 40*, 4951-4959. doi: https://doi.org/10.1016/j.ijhydene.2015.01.101

González-Quijano, D., Pech-Rodríguez, W. J., González-Quijano, J. A., Escalante-García, J. I., Vargas-Gutiérrez, G., Alonso-Lemus, I., & Rodríguez-Varela, F. J. (2015). Electrocatalysts for ethanol and ethylene glycol oxidation reactions. Part II: effects of the polyol synthesis conditions on the characteristics and catalytic activity of Pt-Ru/C anodes. *International Journal of Hydrogen Energy 40*, 17291-17299. doi: http://dx.doi.org/10.1016/j.ijhydene.2015.06.154

Goor, Meital, Menkin, Svetlana, & Peled, Emanuel. (2019). High power direct methanol fuel cell for mobility and portable applications. *International Journal of Hydrogen Energy 44*, 3138-3143. doi: https://doi.org/10.1016/j.ijhydene.2018.12.019

Guha, Abhishek, Lu, Weijie, Zawodzinski, Thomas A., & Schiraldi, David A. (2007). Surface-modified carbons as platinum catalyst support for PEM fuel cells. *Carbon 45*, 1506-1517. doi: https://doi.org/10.1016/j.carbon.2007.03.023

Guillén-Villafuerte, Olmedo, García, Gonzalo, Arévalo, M. Carmen, Rodríguez, José Luis, & Pastor, Elena. (2016). New insights on the electrochemical oxidation of ethanol on carbon-supported Pt electrode by a novel electrochemical mass spectrometry configuration. *Electrochemistry Communications 63*, 48-51. doi: https://doi.org/10.1016/j.elecom.2015.12.007

He, Chaoxiong, Liang, Yeru, Fu, Ruowen, Wu, Dingcai, Song, Shuqin, & Cai, Rui. (2011). Nanopores array of ordered mesoporous carbons determine Pt's activity towards alcohol electrooxidation. *Journal of Materials Chemistry 21*, 16357-16364. doi: https://doi.org/10.1039/C1JM13423J

Hsu, H Y, & Tongol, B J. (2013). Electrochemical and surface characteristics of carbon-supported

PtSn electrocatalysts for ethanol electro-oxidation: possible application for inkjet ink formulations. *Advances in Natural Sciences: Nanoscience and Nanotechnology 4*, 015012-015017. doi: https://doi.org/10.1088/2043-6262/4/1/015012

Ioroi, Tsutomu, Siroma, Zyun, Yamazaki, Shin-ichi, & Yasuda, Kazuaki. (2019). Electrocatalysts for PEM fuel cells. *Advanced Energy Materials 9*, 1801284-1801294. doi: https://doi.org/10.1002/aenm.201801284

Kuznetsova, Anya, Mawhinney, Douglas B., Naumenko, Viktor, Yates Jr, John T., Liu, J., & Smalley, R. E. (2000). Enhancement of adsorption inside of single-walled nanotubes: opening the entry ports. *Chemical Physics Letters 321*, 292-296. doi: http://dx.doi.org/10.1016/S0009-2614(00)00341-9

Lai, Stanley C. S., Kleijn, Steven E. F., Öztürk, Fatma T. Z., van Rees Vellinga, Vivienne C., Koning, Jesper, Rodriguez, Paramaconi, & Koper, Marc T. M. (2010). Effects of electrolyte pH and composition on the ethanol electro-oxidation reaction. *Catalysis Today 154*, 92-104. doi: https://doi.org/10.1016/j.cattod.2010.01.060

Lakshmi, N., Rajalakshmi, N. , & Dhathathreyan, K. S. . (2006). Functionalization of various carbons for proton exchange membrane fuel cell electrodes: analysis and characterization. *Journal of Physics D: Applied Physics 39*, 2785-2796. doi: https://doi.org/10.1088/0022-3727/39/13/022

Lamy, C., Belgsir, E. M., & Léger, J. M. (2001). Electrocatalytic oxidation of aliphatic alcohols: application to the direct alcohol fuel cell (DAFC). *Journal of Applied Electrochemistry 31*, 799-809. doi: https://doi.org/10.1023/A:1017587310150

Li, Huanqiao, Sun, Gongquan, Cao, Lei, Jiang, Luhua, & Xin, Qin. (2007). Comparison of different promotion effect of PtRu/C and PtSn/C electrocatalysts for ethanol electro-oxidation. *Electrochimica Acta 52*, 6622-6629. doi: http://dx.doi.org/10.1016/j.electacta.2007.04.056

Li, Xiang, An, Li, Chen, Xin, Zhang, Nanlin, Xia, Dingguo, Huang, Weifeng, Chu, Wangsheng, Wu, Ziyu. (2013). Durability enhancement of intermetallics electrocatalysts via N-anchor effect for fuel cells. *Scientific Reports 3*, 3234-3239. doi: https://doi.org/10.1038/srep03234

Lindorfer, Johannes, Rosenfeld, Daniel Cenk, & Böhm, Hans. (2020). 23 - Fuel cells: energy conversion technology. In T. M. Letcher (Ed.), *Future Energy* (Third Edition) (pp. 495-517): Elsevier.

Liu, Zhaolin, Ling, Xing Yi, Su, Xiaodi, & Lee, Jim Yang. (2004). Carbon-supported Pt and PtRu nanoparticles as catalysts for a direct methanol fuel cell. *Journal of Physical Chemistry B 108*, 8234-8240. doi: https://doi.org/10.1021/jp049422b

Lu, Yan, Wang, Wei, Chen, Xiaowei, Zhang, Yuhui, Han, Yanchen, Cheng, Yong, Chen, Xue-Jiao, Liu, Kai, Wang, Yuanyuan, Zhang, Qiaobao, Xie, Shuifen. (2019). Composition optimized trimetallic PtNiRu dendritic nanostructures as versatile and active electrocatalysts for alcohol oxidation. *Nano Research 12*, 651-657. doi: https://doi.org/10.1007/s12274-019-2273-3

Moon, Gun-hee, Park, Yiseul, Kim, Wooyul, & Choi, Wonyong. (2011). Photochemical loading of metal nanoparticles on reduced graphene oxide sheets using phosphotungstate. *Carbon 49*, 3454-3462. doi: https://doi.org/10.1016/j.carbon.2011.04.042

Palma, L. M., Almeida, T. S., Oliveira, V. L., Tremiliosi-Filho, G., Gonzalez, E. R., de Andrade, A. R., Servat, K., Morais, C., Napporn, T.W., Kokoh, K. B. (2014). Identification of chemicals resulted in selective glycerol conversion as sustainable fuel on Pd-based anode nanocatalysts. *RSC Advances 4*, 64476-64483. doi: https://doi.org/10.1039/C4RA09822F

Paul, Michael T. Y., Saha, Madhu S., Qi, Wei Li, Stumper, Juergen, & Gates, Byron D. (2020). Microstructured membranes for improving transport resistances in proton exchange membrane fuel cells. *International Journal of Hydrogen Energy 45*, 1304-1312. doi: https://doi.org/10.1016/j.ijhydene.2019.05.186

Pech-Rodríguez, W. J., González-Quijano, D., Vargas-Gutiérrez, G., Morais, C., Napporn, T. W., & Rodríguez-Varela, F. J. (2017). Electrochemical and in situ FTIR study of the ethanol oxidation reaction on PtMo/C nanomaterials in alkaline media. *Applied Catalysis B: Environmental 203*, 654-662. doi: http://dx.doi.org/10.1016/j.apcatb.2016.10.058

Pech-Rodríguez, W. J., González-Quijano, D., Vargas-Gutiérrez, G., & Rodríguez-Varela, F. J. (2014). Electrophoretic deposition of polypyrrole/Vulcan XC-72 corrosion protection coatings on SS-304 bipolar plates by asymmetric alternating current for PEM fuel cells. *International Journal of Hydrogen Energy 39*, 16740-16749. doi: http://dx.doi.org/10.1016/j.ijhydene.2014.03.209

Pech-Rodríguez, W.J., Gonzalez-Quijano, D., Vargas-Gutierrez, G., Escalante-Garcia, J.I., & Rodriguez-Varela, F.J. (2014). Electrochemical characterization of Pt nanocatalysts supported on functionalized vulcan XC-72 for the EOR. *ECS Transactions 61*, 11-18. doi: https://doi.org/10.1149/06129.0011ecst

Poh, Chee Kok, Lim, San Hua, Pan, Hui, Lin, Jianyi, & Lee, Jim Yang. (2008). Citric acid functionalized carbon materials for fuel cell applications. *Journal of Power Sources 176*, 70-75. doi: http://dx.doi.org/10.1016/j.jpowsour.2007.10.049

Rivera-Lugo, Y., Silva-Carrillo, C., Trujillo-Navarrete, B., Reynoso-Soto, E., Romero-Castañón, T., Lin-Ho, S., Calva-Yañez, J., Paraguay-Delgado, F., Félix-Navarro, R. (2020). Cobalt and copper nanoparticles on partially reduced graphene oxide interlayer spacing carbon nanotubes or carbon black as catalysts for oxygen reduction reaction. *Revista Mexicana De Ingeniería Química 20*, 9. doi: https://doi.org/10.24275/rmiq/Mat961

Rizo, Rubén, Pérez-Rodríguez, Sara, & García, Gonzalo. (2019). Well-defined platinum surfaces for the ethanol oxidation reaction. *ChemElectroChem 6*, 4725-4738. doi: https://doi.org/10.1002/celc.201900600

Scibioh, M. Aulice, Kim, Soo-Kil, Cho, Eun Ae, Lim, Tae-Hoon, Hong, Seong-Ahn, & Ha, Heung Yong. (2008). Pt-CeO_2/C anode catalyst for direct methanol fuel cells. *Applied Catalysis B Environmental 84*, 773-782. doi: http://dx.doi.org/10.1016/j.apcatb.2008.06.017

Shao, Yuyan, Dodelet, Jean-Pol, Wu, Gang, & Zelenay, Piotr. (2019). PGM-free cathode catalysts for PEM fuel cells: a mini-review on stability challenges. *Advanced Materials 31*, 1807615-1807625. doi: https://doi.org/10.1002/adma.201807615

Sikeyi, Ludwe L., Ntuli, Themba D., Mongwe, Thomas H., Maxakato, Nobanathi W., Carleschi, Emanuela, Doyle, Bryan P., Coville, Neil J.,Maubane-Nkadimeng, Manoko S. (2021). Microwave assisted synthesis of nitrogen doped and oxygen functionalized carbon nano onions supported palladium nanoparticles as hybrid anodic electrocatalysts for direct alkaline ethanol fuel cells. *International Journal of Hydrogen Energy 46*, 10862-10875. doi: https://doi.org/10.1016/j.ijhydene.2020.12.154

Silva, J. C. M., De Souza, R. F. B., Parreira, L. S., Neto, E. Teixeira, Calegaro, M. L., & Santos, M. C. (2010). Ethanol oxidation reactions using SnO_2Pt/C as an electrocatalyst. *Applied Catalysis, B: Environmental 99*, 265-271. doi: http://dx.doi.org/10.1016/j.apcatb.2010.06.031

Siller-Ceniceros, A. A., Sánchez-Castro, M. E., Morales-Acosta, D., Torres-Lubian, J. R., Martínez G, E., & Rodríguez-Varela, F. J. (2017). Innovative functionalization of Vulcan XC-72 with Ru organometallic complex: significant enhancement in catalytic activity of Pt/C electrocatalyst for the methanol oxidation reaction (MOR). *Applied Catalysis B: Environmental 209*, 455-467. doi: https://doi.org/10.1016/j.apcatb.2017.03.023

Siller-Ceniceros, Adriana A., Sánchez-Castro, Esther, Morales-Acosta, Diana, Torres-Lubián, José R., Martínez-Guerra, Eduardo, & Rodríguez-Varela, Javier. (2019). Functionalizing reduced graphene oxide with Ru-organometallic compounds as an effective strategy to produce high-performance Pt nanocatalysts for the methanol oxidation reaction. *ChemElectroChem. 6*, 4902-4916.

doi: https://doi.org/10.1002/celc.201901190

Song, S. Q., Zhou, W. J., Zhou, Z. H., Jiang, L. H., Sun, G. Q., Xin, Q., Leontidis, V., Kontous, S., Tsiakaras, P. (2005). Direct ethanol PEM fuel cells: the case of platinum based anodes. *International Journal of Hydrogen Energy 30* 995-1001. doi: https://doi.org/10.1016/j.ijhydene.2004.11.006

Song, Shuqin, He, Chaoxiong, Liu, Jinchao, Wang, Yi, Brouzgou, Angeliki, & Tsiakaras, Panagiotis. (2012). Two-step sequence for synthesis of efficient PtSn@Rh/C catalyst for oxidizing ethanol and intermediate products. *Applied Catalysis B: Environmental 119-120*, 227-233. doi: http://dx.doi.org/10.1016/j.apcatb.2012.02.022

Thompson, Scott D., Jordan, Larry R., & Forsyth, Maria. (2001). Platinum electrodeposition for polymer electrolyte membrane fuel cells. *Electrochimica Acta 46*, 1657-1663. doi: http://dx.doi.org/10.1016/S0013-4686(00)00767-2

Thotiyl, M. M. Ottakam, Kumar, T. Ravi, & Sampath, S. (2010). Pd supported on titanium nitride for efficient ethanol oxidation. *Journal of Physical Chemistry C 114*, 17934-17941. doi: https://doi.org/10.1021/jp1038514

Vesali-Naseh, Masoud, Khodadadi, Abbas Ali, Mortazavi, Yadollah, Alizadeh Sahraei, Ommolbanin, Pourfayaz, Fathollah, & Mosadegh, Sanaz. (2009). Functionalization of carbon nanotubes using nitric acid oxidation and DBD plasma. *Int. J. Chem. Biol. Eng. 3*, 133-136.

Wang, Jiajun, Yin, Geping, Shao, Yuyan, Zhang, Sheng, Wang, Zhenbo, & Gao, Yunzhi. (2007). Effect of carbon black support corrosion on the durability of Pt/C catalyst. *Journal of Power Sources 171*, 331-339. doi: http://dx.doi.org/10.1016/j.jpowsour.2007.06.084

Wang, Li, Wurster, Peter, Gazdzicki, Pawel, Roussel, Manuel, Sanchez, Daniel G., Guétaz, Laure, Jacques, Pierre-André, Gago, Aldo S., Andreas Friedrich, K. (2017). Investigation of activity and stability of carbon supported oxynitrides with ultra-low Pt concentration as ORR catalyst for PEM fuel cells. *Journal of Electroanalytical Chemistry 819*, 312-321. doi: https://doi.org/10.1016/j.jelechem.2017.10.067

Wang, Q., Sun, G. Q., Jiang, L. H., Xin, Q., Sun, S. G., Jiang, Y. X., Chen, S.P., Jusys, Z., Behm, R. J. (2007). Adsorption and oxidation of ethanol on colloid-based Pt/C, PtRu/C and Pt3Sn/C catalysts: In situ FTIR spectroscopy and on-line DEMS studies. *Physical Chemistry Chemical Physics 9*, 2686-2696. doi: https://doi.org/10.1039/B700676B

Wang, Xiaoying, Zhang, Xiaofeng, He, Xiaolei, Ma, Ai, Le, Lijuan, & Lin, Shen. (2015). Facile electrodeposition of flower-Like PMo12-Pt/rGO composite with enhanced electrocatalytic activity towards methanol oxidation. *Catalysts 5*, 1275-1288. doi: https://doi.org/10.3390/catal5031275

Wang, Yun, Ruiz Diaz, Daniela Fernanda, Chen, Ken S., Wang, Zhe, & Adroher, Xavier Cordobes. (2020). Materials, technological status, and fundamentals of PEM fuel cells - a review. *Materials Today 32*, 178-203. doi: https://doi.org/10.1016/j.mattod.2019.06.005

Wang, Zhen-Bo, Yin, Ge-Ping, & Lin, Yong-Ge. (2007). Synthesis and characterization of PtRuMo/C nanoparticle electrocatalyst for direct ethanol fuel cell. *Journal of Power Sources 170*, 242-250. doi: http://dx.doi.org/10.1016/j.jpowsour.2007.03.078

Wnuk, Paweł, & Lewera, Adam. (2020). On-line analysis of ethanol electrochemical oxidation process in a low-temperature direct ethanol fuel cell. *Electrochimica Acta 330*, 135256-135266. doi: https://doi.org/10.1016/j.electacta.2019.135256

Wu, J., Hu, F., Shen, P. K., Li, C. M., & Wei, Z. (2010). One-step preparation of Pt on pretreated multiwalled carbon nanotubes for methanol electrooxidation. *Fuel Cells 10*, 106-110. doi: https://doi.org/10.1002/fuce.200900119

Yang, Guangxing, Zhang, Qiao, Yu, Hao, & Peng, Feng. (2021). Platinum-based ternary catalysts for the electrooxidation of ethanol. *Particuology*. doi: https://doi.org/10.1016/j.partic.2021.01.007

Yang, Yu Jun, & Li, Weikun. (2014). CTAB functionalized graphene oxide/multiwalled carbon nanotube composite modified electrode for the simultaneous determination of ascorbic acid, dopamine, uric acid and nitrite. *Biosensors and Bioelectronics 56*, 300-306. doi: http://dx.doi.org/10.1016/j.bios.2014.01.037

Yin, Shibin, Luo, Lin, Xu, Cheng, Zhao, Yulong, Qiang, Yinghuai, & Mu, Shichun. (2012). Functionalizing carbon nanotubes for effective electrocatalysts supports by an intermittent microwave heating method. *Journal of Power Sources 198*, 1-6. doi: http://dx.doi.org/10.1016/j.jpowsour.2011.09.061

Yin, Shibin, Shen, Pei Kang, Song, Shuqin, & Jiang, San Ping. (2009). Functionalization of carbon nanotubes by an effective intermittent microwave heating-assisted HF/H_2O_2 treatment for electrocatalyst support of fuel cells. *Electrochimica Acta 54*, 6954-6958. doi: http://dx.doi.org/10.1016/j.electacta.2009.07.009

Youssry, Mohamed, Al-Ruwaidhi, Maisa, Zakeri, Mahdiyeh, & Zakeri, Mohadese. (2020). Physical functionalization of multi-walled carbon nanotubes for enhanced dispersibility in aqueous medium. *Emergent Materials 3*, 25-32. doi: http://dx.doi.org/10.1007/s42247-020-00076-3

Zhang, Chaoli, Zhu, Aimei, Huang, Rong, Zhang, Qiugen, & Liu, Qinglin. (2014). Hollow nanoporous Au/Pt core-shell catalysts with nanochannels and enhanced activities towards electro-oxidation of methanol and ethanol. *International Journal of Hydrogen Energy 39*, 8246-8256. doi: http://dx.doi.org/10.1016/j.ijhydene.2014.03.193

Zhang, Weiyu, Yang, Yong, Huang, Bolong, Lv, Fan, Wang, Kai, Li, Na, Luo, Mingchuan, Chao, Yuguang, Li, Yingjun, Xu, Zhikun, Qin, Yingnan, Yang, Wenxiu, Zhou, Jinhui, Du, Yaping, Su, Dong, Guo, Shaojun. (2019). Ultrathin PtNiM (M = Rh, Os, and Ir) nanowires as efficient fuel oxidation electrocatalytic materials. *Advanced Materials 31*, 1805833-1805842. doi: https://doi.org/10.1002/adma.201805833

Zhang, Xiao, Yang, Ping, & Jiang, San Ping. (2021). Pd nanoparticles assembled on Ni- and N-doped carbon nanotubes towards superior electrochemical activity. *International Journal of Hydrogen Energy 46*, 2065-2074. doi: https://doi.org/10.1016/j.ijhydene.2020.10.096

Zhou, W. J., Song, S. Q., Li, W. Z., Sun, G. Q., Xin, Q., Kontou, S., Pouliamitis, K., Tsiakaras, P. (2004). Pt-based anode catalysts for direct ethanol fuel cells. *Solid State Ionics 175*, 797-803. doi: http://dx.doi.org/10.1016/j.ssi.2004.09.055

Zhou, Zhi-You, Wang, Qiang, Lin, Jian-Long, Tian, Na, & Sun, Shi-Gang. (2010). In situ FTIR spectroscopic studies of electrooxidation of ethanol on Pd electrode in alkaline media. *Electrochimica Acta 55*, 7995-7999. doi: http://dx.doi.org/10.1016/j.electacta.2010.02.071